ELSEVIER

Volume 183, Issue 11, November 2010

JOURNAL OF SOLID STATE CHEMISTRY

www.elsevier.com/locate/jssc

CONTENTS

Abstracted/indexed in BioEngineering Abstracts, Chemical Abstracts, Coal Abstracts, Current Contents/Physics, Chemical, & Earth Sciences, Engineering Index, Research Alert, SCISEARCH, Science Abstracts, and Science Citation Index. Also covered in the abstract and citation database SCOPUS®. Full text available on ScienceDirect®.

Regular Articles

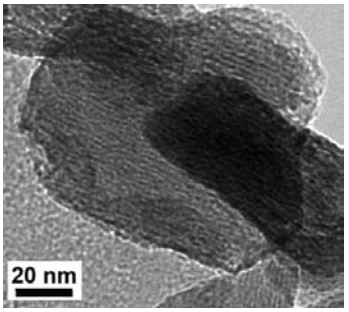

Ordered mesoporous Mg–Al MMOs can be obtained through the calcination of P123-templated Mg–Al–CO_3 LDHs. The pore diameter is 2.2 nm. At the presence of ibuprofen, the Mg–Al MMOs can recover to Mg–Al–IBU LDHs, based on its "remember effect".

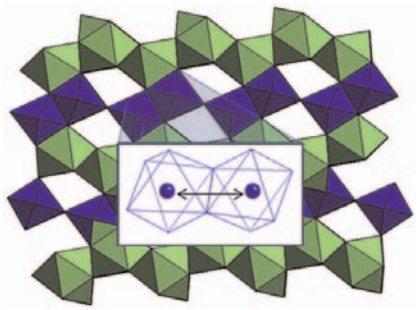

The energetics of three lanthanum tantalates were investigated by the high-temperature oxide melt solution calorimetry. The enthalpies of formation from the oxides were calculated from the enthalpies of drop solution to be -87.1 ± 9.6, -94.9 ± 8.8, and -93.1 ± 8.7 kJ/mol for $La_2Ta_2O_7(OH)_2$, $LaTaO_4$ (850 °C), and $LaTaO_4$ (1200 °C), respectively. These results indicate that the intermediate phase, $LaTaO_4$ (850 °C), is the most stable in energy.

Regular Articles—Continued

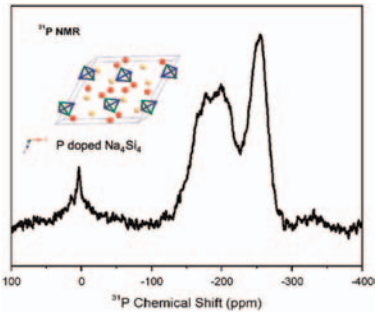

P-doped Na_4Si_4 has been prepared and Raman spectroscopy and ^{29}Si, ^{23}Na, and ^{31}P multinuclear NMR show that P dopes into both crystallographic sites for Si.

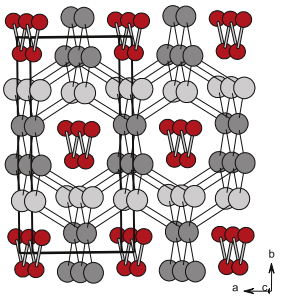

A new phase, Li_2Al, has been discovered in the binary Li–Al system. The structure of orthorhombic Li_2Al is closely related to that of the established monoclinic phase Li_9Al_4.

Continued

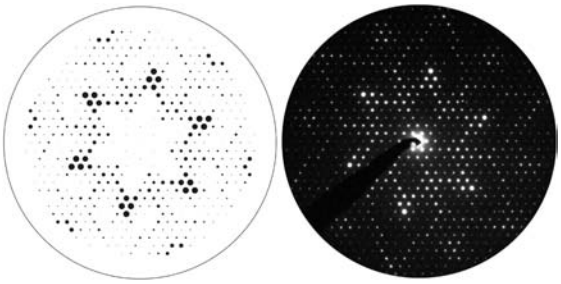

The new ternary pnictides $Er_{12}Ni_{30}P_{21}$ and $Er_{13}Ni_{25}As_{19}$ have been synthesized from the elements. They crystallize with hexagonal structures determined from single-crystal X-ray data. The compounds belong to a large family of structures with a metal–metalloid ratio of 2:1. HRTEM investigations were conducted to probe for local ordering of the disordered structure at the nanoscale.

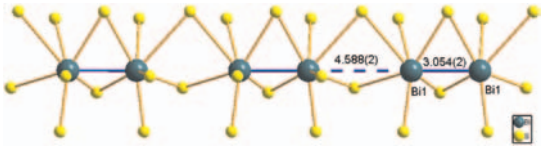

Two new bismuth sulfides $Bi_3In_4S_{10}$ and $Bi_{14.7}In_{11.3}S_{38}$ have been synthesized and characterized. The figure is the arrangement of Bi1 atoms along the *b* direction with alternating short and long distances (Å) in $Bi_3In_4S_{10}$.

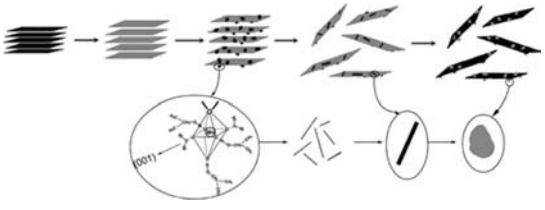

Manganese oxyhydroxide nanocrystals have been successfully attached onto the graphene sheets via an oriented attachment and dissolution-crystallization process, forming a nanocomposite with unusual catalytic capabilities.

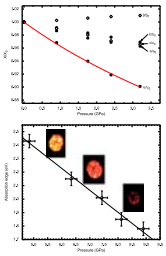

(up) Structural evolutions of Tl_2MoO_4 in the low-pressure phase. (Down) Optical properties of the high-pressure phase as a function of pressure.

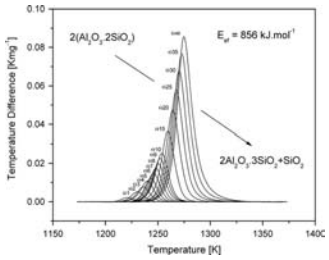

Kinetics of crystallization of Al–Si spinel from calcined kaolin was investigated by the DTA using the Kissinger kinetic approach. The apparent activation energy and morphology parameter of the process is 856 ± 2 kJ mol^{-1} and 3.08 ± 0.03, respectively.

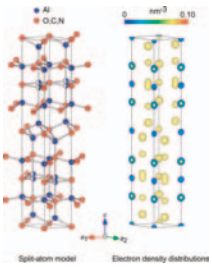

A new oxycarbonitride discovered in the Al–O–C–N system, $Al_5(O_{1.4}C_{2.1}N_{0.5})$. The crystal is an inversion twin, and hence the structure is represented by a split-atom model. The three-dimensional electron density distributions are determined by the maximum-entropy methods-based pattern fitting, being consistent with the disordered structural model.

Hydrothermal synthesis and electrochemical performance of NiO microspheres with different nanoscale building blocks
Ling Wang, Yanjing Hao, Yan Zhao, Qiongyu Lai and Xiaoyun Xu
Page 2576

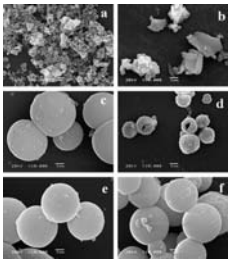

Fig. 5 is the SEM image of NiO that was prepared in the different hydrothermal reaction temperatures. It showed that reaction temperature played a crucial role for the morphology of products.

Series of compositions $Bi_2(M'_xM_{1-x})_4O_9$ (M', M = Al, Ga, Fe; $0 \le x \le 1$) with mullite-type crystal structure: Synthesis, characterization and $^{18}O/^{16}O$ exchange experiment
T. Debnath, C.H. Rüscher, P. Fielitz, S. Ohmann and G. Borchardt
Page 2582

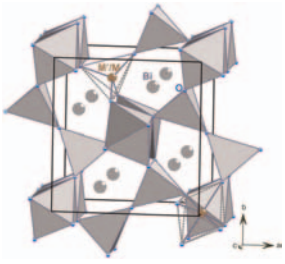

Fig. Perspective view of the mullite-type $Bi_2(M'_xM_{1-x})_4O_9$ unit cell (M', M = Al, Ga, Fe).

Synthesis, structural characterization and Li^+ ion conductivity of a new vanado-molybdate phase, $LiMg_3VMo_2O_{12}$
Lisa J. Gillie, Sharon A. de Souza, Denis Sheptyakov, Nik Reeves-McLaren, Denis Pasero and Anthony R. West
Page 2589

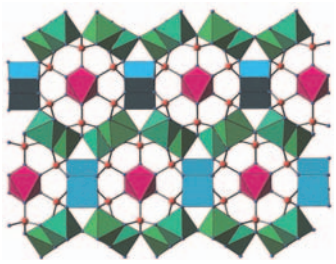

A new vanado-molybdate $LiMg_3VMo_2O_{12}$ has been synthesized and the crystal structure determined. Ionic conductivity measurements show the presence of a phase transition, at 500–600 °C. A large decrease in activation energy for Li^+ ion conductivity occurs at the phase transition and the high temperature structure is a good Li^+ ion conductor.

Effect of biphase on dielectric properties of Bi-doped lead strontium titanate thin films
X.T. Li, P.Y. Du, Y.L. Zhao, Y. Tu, J.L. Dai, W.J. Weng, G.R. Han and C.L. Song
Page 2598

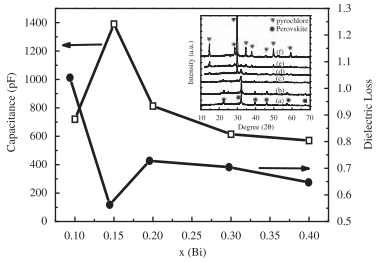

The Bi-doped $Pb_{0.4}Sr_{0.6}TiO_3$ (PST) thin films prepared by the sol–gel method showed a PST/$Bi_2Ti_2O_7$ biphase structure for $0.2 < x < 0.4$, and had the low dielectric capacitance and dielectric loss.

Infrared spectroscopic study of the local structural changes across the metal insulator transition in nickel-doped $GdBaCo_2O_{5.5}$
P. Yasodha, M. Premila, A. Bharathi, M.C. Valsakumar, R. Rajaraman and C.S. Sundar
Page 2602

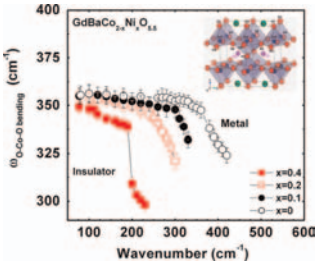

Softening of the bending mode across T_{MIT}.

Controllable fabrication of platinum nanospheres with a polyoxometalate-assisted process
Guoying Sun, Qiuyu Li, Rui Xu, Jianmin Gu, Mingliang Ju and Enbo Wang
Page 2609

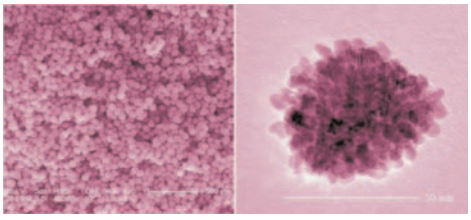

Large-scale Pt nanospheres were synthesized through a polyoxometalate-assisted process, and exhibited good electrocatalytic activity towards the oxidation of methanol, making them promising for applications in fuel cells.

Continued

Synthesis and phase width of new quaternary selenides $Pb_xSn_{6-x}Bi_2Se_9$ ($x = 0$–4.36)

Kuei-Bo Chen and Chi-Shen Lee

Page 2616

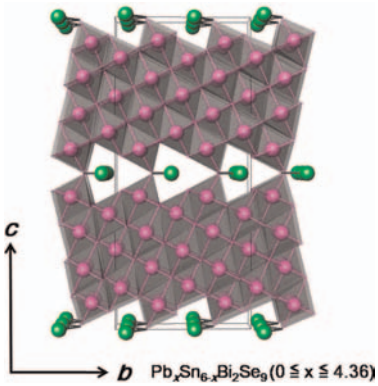

SYNOPSIS TOC New quaternary selenides, $Pb_xSn_{6-x}Bi_2Se_9$ ($x = 0$–4.36), were synthesized and their structure consisting layers of seven octahedra wide slabs expanding along the direction [0 1 0].

Magnetic dilution of the iron sublattice in $CoFe_{2-x}Sc_xO_4$ ($0 \leq x \leq 1$)

C. Lefevre, F. Roulland, N. Viart, J.M. Greneche and G. Pourroy

Page 2623

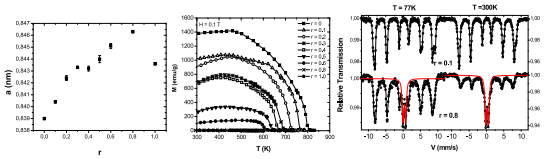

Evolution of the cell parameters, the magnetic properties and the Mössbauer spectra in $CoFe_{2-r}Sc_rO_4$ ($0 \leq r \leq 1$).

Two-step synthesis of Bi_2Te_3–Te nanoarrays with sheet–rod multiple heterostructure

Yuan Deng, Zhiwei Zhang, Yao Wang, Meng Yang and Rongmin Wang

Page 2631

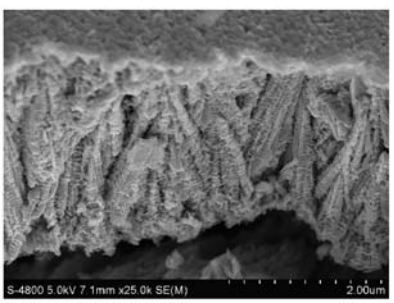

Bi_2Te_3–Te arrays with sheet–rod multiple heterostructure were obtained in a large scale using Te nanorod arrays as the in-situ templates under the solvothermal process.

Pressure-induced structural transformations in lanthanide titanates: La_2TiO_5 and Nd_2TiO_5

F.X. Zhang, J.W. Wang, M. Lang, J.M. Zhang and R.C. Ewing

Page 2636

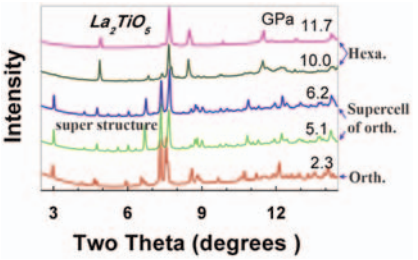

At high pressures, La_2TiO_5 and Nd_2TiO_5 transform from the orthorhombic phase to an $a \times b \times 2c$ superlattice of the orthorhombic structure and then to a hexagonal high-pressure phase.

Hydrazine-hydrothermal method to synthesize three-dimensional chalcogenide framework for photocatalytic hydrogen generation

Yi Liu, Pushkar D. Kanhere, Chui Ling Wong, Yuefeng Tian, Yuhua Feng, Freddy Boey, Tom Wu, Hongyu Chen, Tim J. White, Zhong Chen and Qichun Zhang

Page 2644

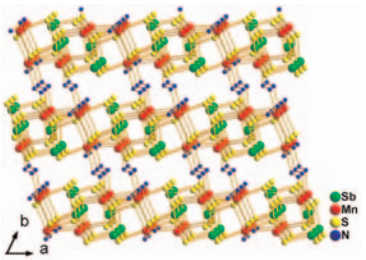

A novel chalcogenide, $[Mn_2Sb_2S_5(N_2H_4)_3]$ (**1**), synthesized by hydrazine-hydrothermal method, has a band gap of about ~2.09 eV and displays photocatalytic behaviors under visible light irradiation.

Crystal structure and magnetic properties of $Na_2Ni^{II}(HPO_3)_2$

Wassim Maalej, Serge Vilminot, Zakaria Elaoud, Tahar Mhiri and Mohamedally Kurmoo

Page 2650

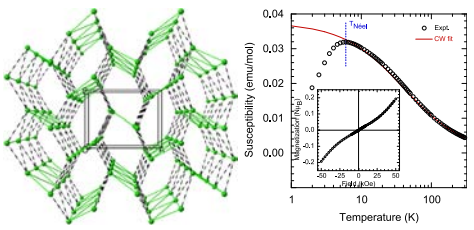

The structure of $Na_2Ni(HPO_3)_2$ consists of zig-zag chains of NiO_6 octahedra bridged by two HPO_3^{2-} and the chains are further connected through HPO_3^{2-} to four nearest chains to form a three dimensional framework, delimiting intersecting tunnels in which the sodium ions are located. It orders antiferromagnetically at 6 K.

Dual graphs realized in the compounds di-μ_3-4-mercaptopyridine catena-di-μ_2-iodo-di-μ_3-iodo-μ_4-iodo penta copper(I) and di-μ_3-4-mercaptopyridine-di-catena-iodo-di-μ_3-iodo tri copper(I)
Ehsan Jalilian and Sven Lidin
Page 2656

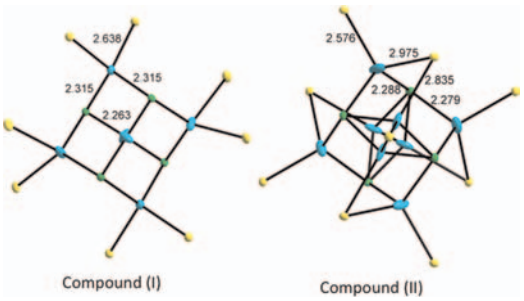

A comparison of the central core in both compounds.

Nitrogen vacancy and ferromagnetism in Cr-doped GaN: First-principles calculations
Yanlu Li, Weiliu Fan, Honggang Sun, Xiufeng Cheng, Pan Li, Xian Zhao and Minhua Jiang
Page 2662

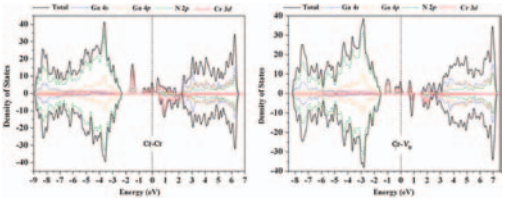

Nitrogen defects and their effect on the ferromagnetism in Cr-doped GaN were investigated by first-principles. Given are the PDOS of $Ga_{36}N_{36}$ with one Cr–Cr pair and one complex of Cr–V_N.

In-situ synthesis of magnetic ($NiFe_2O_4$/CuO/FeO) nanocomposites
Manish Srivastava, Animesh K. Ojha, S. Chaubey and Jay Singh
Page 2669

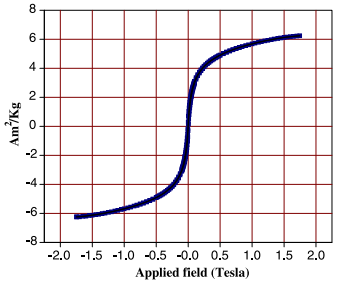

Magnetic nanocomposites containing ($NiFe_2O_4$/CuO/FeO) phases having particle size ~17 nm were synthesized by a sol–gel method. The synthesized nanocomposites exhibit ferromagnetic nature with small value of coercivity.

Hydrothermal crystal growth of the potassium niobate and potassium tantalate family of crystals
Matthew Mann, Summer Jackson and Joseph Kolis
Page 2675

Magnetic properties and structural transitions of orthorhombic fluorite-related compounds Ln_3MO_7 (Ln = rare earths, M = transition metals)
Makoto Wakeshima and Yukio Hinatsu
Page 2681

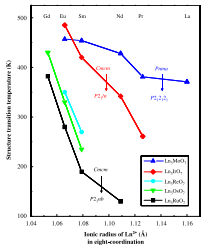

Magnetic properties and structural transitions of ternary rare-earth transition-metal oxides Ln_3MO_7 (Ln = rare earths, M = transition metals) were investigated. In this study, we prepared a series of molybdates Ln_3MoO_7 (Ln = La ~ Gd). These compounds show a phase transition from the space group $P2_12_12_1$ to *Pnma* in the temperature range between 370 and 710 K. Their magnetic properties were characterized by magnetic susceptibility and specific heat measurements from 0.4 to 400 K. The results of Ln_3MoO_7 were compared with the magnetic properties and structural transitions of Ln_3MO_7 (M = Nb, Ru, Sb, Ta, Re, Os, or Ir).

***B*-site ordered perovskite $LaSrMnNbO_6$: Synthesis, structure and antiferromagnetism**
Tao Yang, Tyché Perkisas, Joke Hadermann, Mark Croft, Alexander Ignatov and Martha Greenblatt
Page 2689

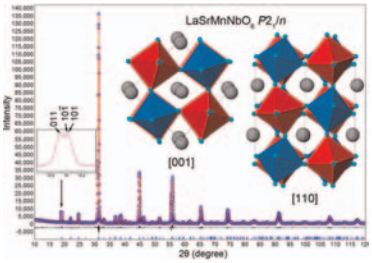

An ordered double perovskite, $LaSrMnNbO_6$ has been synthesized in the monoclinic space group $P2_1/n$. The Mn^{2+} and Nb^{5+} ions, whose valence states are confirmed by X-ray absorption near-edge spectroscopy, are ordered over the *B*-site. The magnetic susceptibility data indicate long-range antiferromagnetic ordering at T_N = 8 K.

Continued

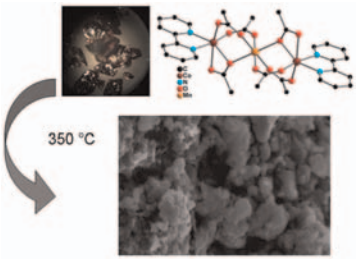

The novel heterometallic complexes $[M_2Mn(OAc)_6(bpy)_2]$ (M = Cu, Co, Zn, bpy = 2,2′-bipyridyl) were isolated and used as precursors for low-temperature synthesis of binary oxides. Single crystal X-ray diffraction, FTIR, TG/DTA/DTG, TPD-MS, PXRD, SEM/EDX analysis was performed on complexes and powders.

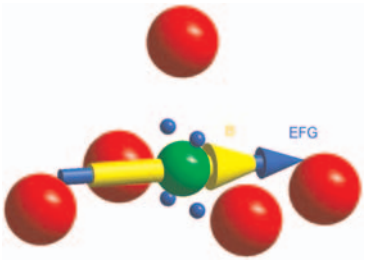

Mössbauer spectrum detects ordering of d_{xz} orbitals of $Fe^{II}O_5$ via the electric-field gradient (EFG) of the orbital, which makes the main component of the total EFG parallel with the magnetic moment B.

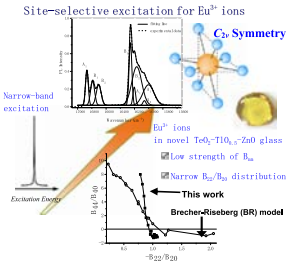

Crystal fields parameters B_{nm} of Eu^{3+} ions (strength, distribution) in novel TeO_2–$TlO_{0.5}$–ZnO glass system.

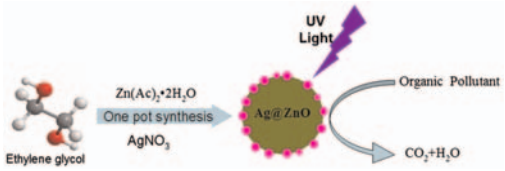

A "one-pot" strategy was developed for preparing the Ag/ZnO microspheres in ethylene glycol. The composites exhibited superior photocatalytic performance for photodegradation of Rhodamine B dye in water.

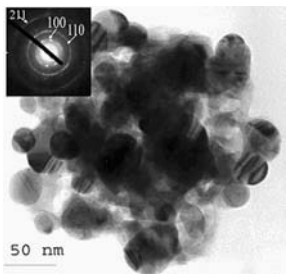

A simple one step process for the preparation of the rare earth silicates with the structure of apatite under a mild condition (230 °C) is presented. The process is based on the hydrothermal synthesis and the obtained powder materials are pure, high crystalline and with nanosize.

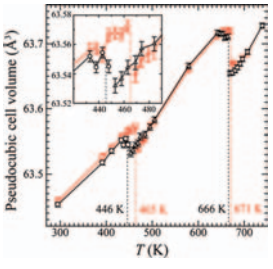

Changes in pseudocubic cell volume of an $Na_{0.5}K_{0.5}NbO_3$ as a function of temperature; the inset is an enlargement near the transition between the orthorhombic and tetragonal forms.

Corrigendum

Corrigendum to "Synthesis, structures, and phase transitions of barium bismuth iridium oxide perovskites Ba_2BiIrO_6 and $Ba_3BiIr_2O_9$" [J. Solid State Chem. 183 (2010) 727–735]

Chris D. Ling, Brendan J. Kennedy, Qingdi Zhou, Jarrah R. Spencer and Maxim Avdeev

Page 2739